*Kovove Mater.* 64 2026 61–70
DOI: 10.31577/km.2026.2.61


# Brittle fracture resistance determined by Charpy impact test of aged and hydrogen-charged 9Cr-1Mo (T91) heat-resistant steel

Ladislav Falat[1]*, Lucia Čiripová[1], Viera Homolová[1], Róbert Džunda[1], Michal Besterci[1]

[1] *Institute of Materials Research of the Slovak Academy of Sciences, Watsonova 47, 04001 Košice, Slovak Republic*

Received 3 March 2026, received in revised form 23 March 2026, accepted 7 May 2026

**Abstract**

In this work the effects of long-term ageing of 9Cr-1Mo (T91) heat-resistant steel on its dynamic hydrogen embrittlement resistance in impact loading conditions were investigated. Altogether three heat-treated material states were studied, namely the initial normalized and tempered (N&T) state, i.e., 1050 °C/0.5 h + 750 °C/1 h and two long-term aged states, i.e., 600 °C/5000 h and 650 °C/5000 h. Charpy V-notch (CVN) impact bending tests were performed at room temperature for all the heat-treated material states in conditions either without or with electrochemical hydrogen charging. A brittle fracture resistance of the investigated material in individual material conditions was evaluated by the determination of *Embrittlement Index* (EI) values in terms of relative changes in CVN impact toughness with respect to variously selected initial and final material conditions. This approach enabled to differentiate the effects of long-term ageing, hydrogen charging, and their mutual superposition on the resulting brittle fracture resistance. The obtained results indicated excellent brittle fracture resistance of studied T91 steel in both the aged and hydrogen-charged material states at impact loading conditions.

K e y w o r d s: 9Cr-1Mo steel, ageing, cathodic hydrogen charging, impact toughness, fracture micro-mechanism

## 1. Introduction

Grade 91 ferritic-matrix heat-resistant steel was developed during the 1980s by the Oak Ridge National Laboratory (ORNL, Tennessee, USA) for the use in high-temperature service conditions of advanced power-engineering equipment [1]. It represents a modified 9Cr-1Mo steel with an optimized chemical composition of alloying elements (0.06 % Nb, 0.2 % V, and 0.05 % N) resulting after the normalizing and tempering (N&T) heat treatment in tempered martensitic microstructure with strengthening precipitates of $M_{23}C_6$ (M = Cr, Fe, Mo) and MX (M = V, Nb, X = C, N) secondary phases [2–5]. The grade 91 steel recommended application temperature lays in the range 590–600 °C for long-term operation. Although during the several last decades further generations of higher-alloyed creep-strength enhanced ferritic (CSEF) grades of tempered martensitic steels with increased creep strength have been developed (e.g. P/T92, C/FB2, E911, MARBN, G115, SAVE12, etc.), the traditional grade 91 steel still remains commercially the highly demanded ferritic boiler steel thanks to its excellent long-term thermal stability with respect to the microstructure and properties in high-temperature creep conditions. The alloying of grade 91 steel with 9 wt.% Cr makes this steel self-quenchable by cooling in air from the austenitization temperature lying above the $A_{c3}$ ferrite-to-austenite phase transformation temperature during normalizing [6, 7]. Subsequent subcritical tempering below the $A_{c1}$ phase transformation temperature assures sufficient relief of thermal and transformation residual stresses and formation of more stable tempered martensitic microstructure with ferrite solid solution matrix and secondary phase precipitates of intergranular Cr-rich $M_{23}C_6$ carbides and intragranular (V,Nb)(C,N) carbonitrides. These minor secondary phases represent the most important precipitation strengthening phases in grade 91 steel [8–10]. Further alloying addition of

*Corresponding author: e-mail address: lfalat@saske.sk

This article is distributed under the terms of the Creative Commons Attri-bution-NonCommercial 4.0 International Public License (CC BY-NC 4.0).

1 wt.% Mo is primarily intended for achieving an efficient solid solution strengthening of the Fe-based ferritic matrix. However, such a high content of molybdenum exceeds its solubility limit in the ferrite phase which subsequently results in the precipitation of $Fe_2Mo$-based intermetallic Laves phase during long-term ageing in laboratory or service conditions [11–15]. As the Laves phase precipitation removes the Mo atoms from solid solution, consequently the solid solution strengthening effect of Mo is reduced during long-term ageing. However, the particles of Laves phase contribute to the precipitation strengthening before the coarsening of the Laves phase occurs. On the other hand, the coarsening of intermetallic Laves phases in 9Cr heat-resistant steels is generally considered the main reason for degradation of their impact toughness and the increase of notch sensitivity. During several last decades, numerous studies about microstructure evolution and mechanical properties of 9Cr heat-resistant steels including their creep strength performance as well as hydrogen embrittlement (HE) sensitivity in static or quasi-static mechanical loading conditions have been widely performed and reported, e.g. [16–22]. However, the studies related to the investigation of HE susceptibility of structural steels in impact loading conditions are still rather limited, e.g. [23–25].

Our current work is focused on the investigation of brittle fracture resistance of traditional T91 heat-resistant steel exposed to long-term ageing and room-temperature electrochemical hydrogenation in order to quantify and discuss partial and superimposed effects of applied ageing and hydrogen-charging conditions on resulting mechanical responses by impact loading. The obtained results on microstructure-property relationships are correlated with observed microstructures and fracture micro-mechanisms. Microstructural conditionality of brittle fracture resistance of long-term aged and cathodically hydrogen-charged T91 heat-resistant steel in impact loading conditions is analyzed and discussed.

## 2. Experimental material and procedures

The as-received T91 material was in the form of commercial steel tube with dimensions of 38 mm outer diameter and 5.6 mm wall thickness. The elemental chemical composition of the tube is given in Table 1.

The initial quality heat treatment of the tube consisted of normalizing and tempering (N&T) at 1050 and 750 °C, respectively (see scheme in Fig. 1). Three tube segments with individual lengths of 70 mm were cut for further experimental work. One tube segment in the initial N&T material condition was considered the reference material state.

The second and third tube segments were subjected to long-term ageing for 5000 hours at 600 and 650 °C, respectively, to produce the long-term aged material states simulating the material degradation during high temperature operation. From each tube segment in individual material condition, six sub-sized CVN impact toughness specimens with half thickness were manufactured due to dimensional restrictions related to the actual wall thickness of the tube. The sampling orientation and the geometric-dimensional

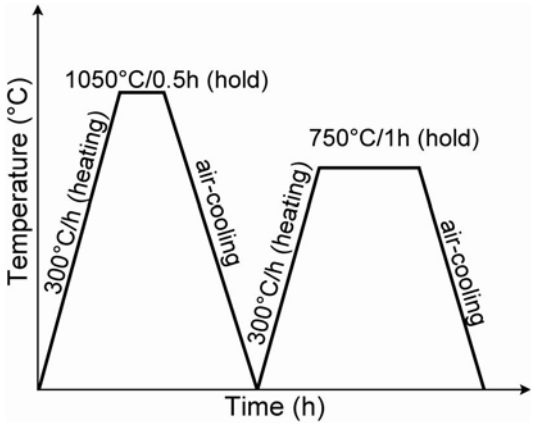


Fig. 1. Scheme of the quality heat treatment for T91 steel tubes.

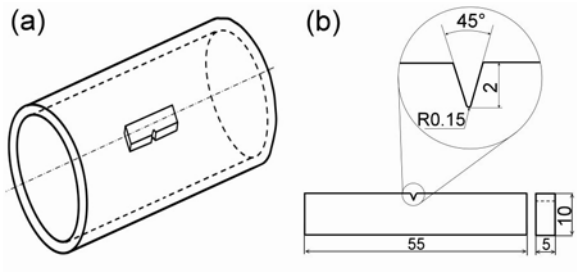


Fig. 2. Sampling of CVN impact toughness specimens from the steel tube (a) and schematic representation of sub-sized CVN specimen (b).

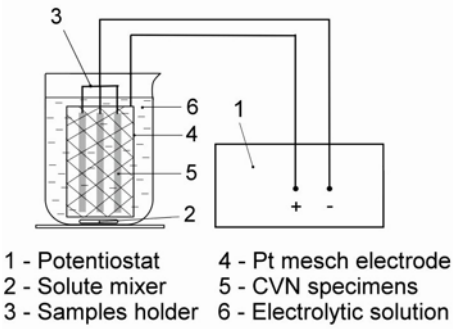


Fig. 3. Experimental set-up for cathodic hydrogen charging of the CVN impact toughness test specimens.

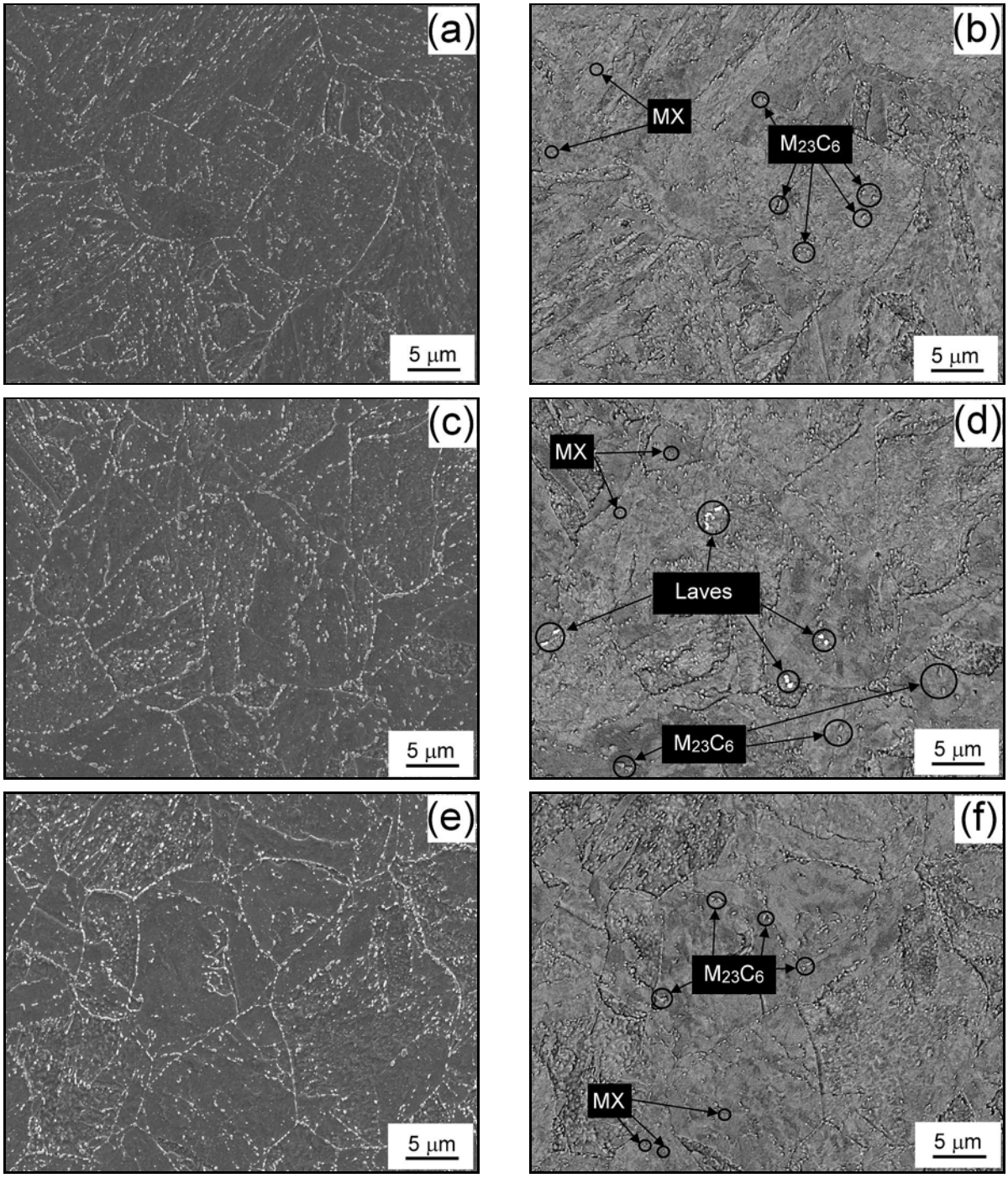


Fig. 4. SEM microstructures of heat-treated material states of T91 material: (a) N&T state, SE mode, (b) N&T state, BSE mode, (c) 600 °C/5000 h state, SE mode, (d) 600 °C/5000 h state, BSE mode, (e) 650 °C/5000 h state, SE mode, and (f) 650 °C/5000 h state, BSE mode.

characteristics of the CVN impact toughness specimens are shown in Fig. 2.

The prismatic bodies of the specimens were produced by conventional grinding machining, whereas the notches were manufactured by spark erosion in order to assure precise notch geometry. The CVN impact toughness tests were carried out for all prepared material states (N&T, 600 °C/5000 h, and 650 °C/5000 h) in conditions without and with subsequent electrochemical hydrogen charging.

The electrochemical hydrogenation of produced CVN impact toughness test specimens was carried out in a solution of 1 M HCl with 0.05M $N_2H_6SO_4$ applying a current density of 200 A $m^{-2}$ for 24 hours at ambient temperature. For each individual material state, three CVN impact toughness specimens were tested

Table 1. Chemical composition of T91 tube under investigation

| C | N | Si | Mn | P | S | Cr | Mo | Ni | Al | V | Nb | Fe |
|---|---|---|---|---|---|---|---|---|---|---|---|---|
| 0.092 | 0.045 | 0.39 | 0.44 | 0.011 | 0.003 | 8.68 | 0.92 | 0.25 | 0.015 | 0.2 | 0.064 | balance |

and the average CVN impact toughness values were evaluated. The schematic set-up of electrochemical hydrogen charging procedure is visualized in Fig. 3.

The embrittlement sensitivity characterizing the effects of applied long-term aging and electrolytic hydrogenation on the brittle-fracture resistance of the studied material was determined by the calculation of the embrittlement index (EI) according to the following equation Eq.(1):

$$\mathrm{EI_{CVN}} = ((\mathrm{CVN_0} - \mathrm{CVN_X})/\mathrm{CVN_0}) \times 100\,\%, \quad (1)$$

where $\mathrm{CVN_0}$ and $\mathrm{CVN_X}$ are the values of Charpy V-notch impact toughness of two individual material states. The subscripts "0" and "X" refer to the states selected as initial and final, respectively [26].

The microstructural and fractographic analyses of the investigated material states were carried out using conventional scanning electron microscopy (SEM) in combination with energy-dispersive X-ray (EDX) spectrometry. Temperature dependence of phase composition of studied material was determined by thermodynamic calculations using *Thermo-Calc software* and non-commercial thermodynamic database STEEL16 developed by Dr. A. Kroupa (IPM ASCR, Brno, Czech Republic) in order to predict evolution of equilibrium phases during long-term ageing and to support experimental findings.

## 3. Results and discussion

Figure 4 shows SEM microstructures of studied T91 material in individual heat-treated material states without application of hydrogen charging. The SEM microstructures are presented in the secondary electrons (SE) mode in Figs. 4a,c,e. In addition, the same microstructural regions are also visualized using backscattered electrons (BSE) mode in Figs. 4b,d,f. The SE imaging mode in SEM is conventionally used for the detailed morphological analyses of material microstructures, whereas SEM microstructural analyses using the BSE imaging mode are highly sensitive on average atomic number of a phase, often referred to as Z-contrast imaging. Thus the BSE visualization mode in SEM has been widely adopted in several research studies of 9Cr heat-resistant steels, e.g., [27–30] to differentiate between the $M_{23}C_6$ chromium-rich carbides with relatively lower average atomic number and intermetallic Laves phases (e.g. $Fe_2Mo$ or $Fe_2W$) with significantly higher average atomic numbers. Representative EDX spectra for individual phases, i.e. ferrite solid solution matrix, Cr-rich $M_{23}C_6$ carbide, $Fe_2Mo$ based Laves phase, and MX (V,Nb)(C,N) carbo-nitride occurring in studied T91 steel in long-term aged material condition (600 ℃/5000 h) are shown in Fig. 5.

By comparison of SEM images recorded in SE visualization mode (Figs. 4a,c,e), it can be concluded that the microstructures related to individual material states do not differ significantly from each other which clearly demonstrates a high thermal stability of T91 steel microstructure under high-temperature ageing conditions. The sizes and morphologies of individual microstructural features, i.e. the grains, subgrains (i.e. tempered martensitic laths), and secondary phase precipitates are very similar for all the heat-treated material states, although a certain grain growth and precipitate coarsening are distinguishable in long-term aged material states compared with the initial N&T material state. The observed grain growth and precipitate coarsening in long-term aged (600 ℃/5000 h and 650 ℃/5000 h) material states have occurred due to thermally-activated diffusional processes leading to the reduction of total system free energy, specifically by minimizing the interfacial energy associated with grain boundaries and particle/matrix interfaces [31]. Grain growth and particle coarsening occur at the expense of the smallest grains and precipitates which are gradually absorbed by the larger grains and precipitates.

On the other hand, the SEM images of studied T91 steel material states recorded in the BSE visualization mode (Figs. 4b,d,f) are presented to enable phase differentiation between the precipitates varying vastly in their average atomic numbers, such as the $M_{23}C_6$ chromium-rich carbides and intermetallic Laves phase. From performed observations it can be concluded that the $Fe_2Mo$ based Laves phase with its sharp bright contrast occurred only after long-term ageing at 600 ℃ for 5000 hours. In comparison with the $Cr_{23}C_6$ based carbides, significant coarsening of the Laves phase has been observed, although its occurrence within the microstructure was rather scarce (Fig. 4d). This observation correlates well with low molybdenum content in T91 steel as shown in Table 1. Moreover, at 650 ℃ no Laves phase precipitates have been observed (Fig. 4f). This observation can be supported by thermodynamic calculations presented in Fig. 6 indicating the occurrence of stable phases in T91 steel in dependence of temperature. According to the phase diagrams, the Laves phase solvus temperature for

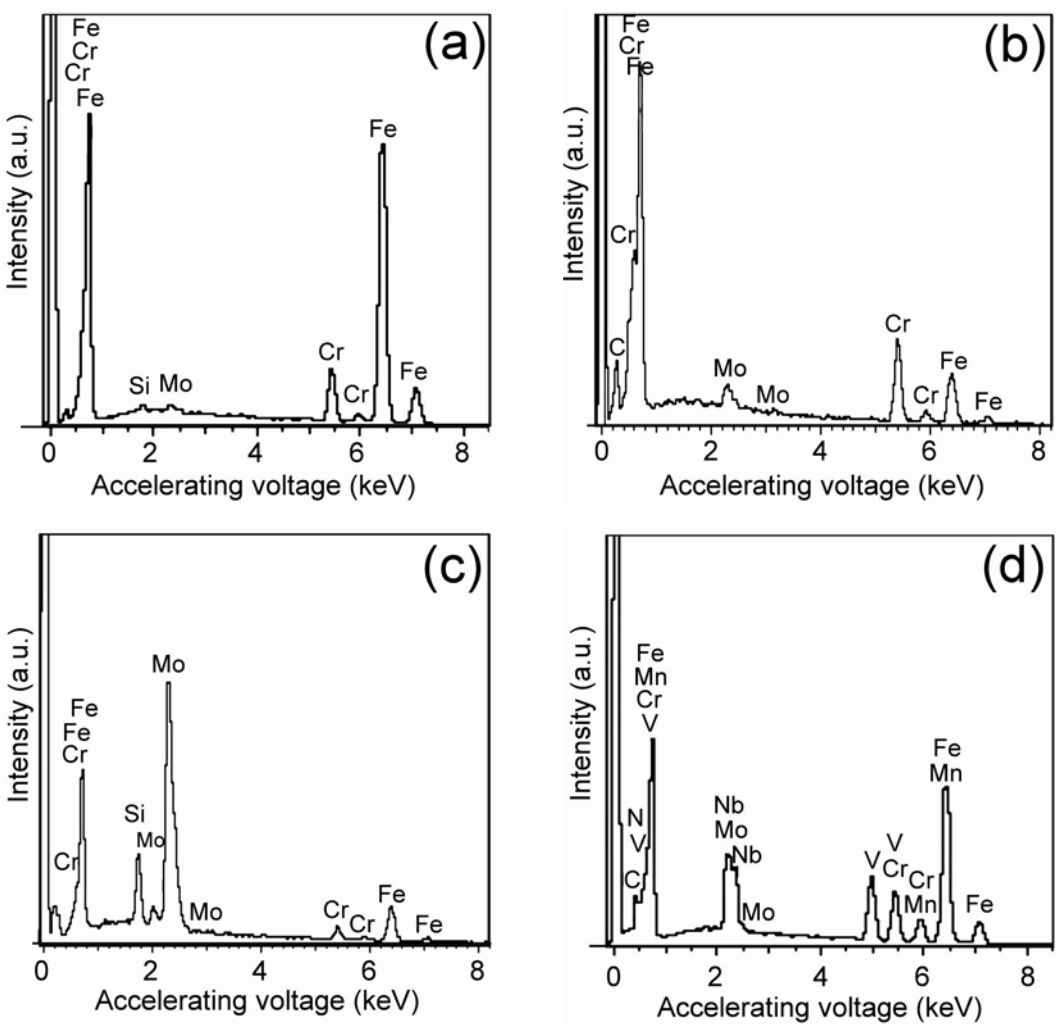


Fig. 5. Typical EDX spectra of individual phases occurring in studied T91 steel after long-term ageing at 600 ℃ for 5000 h: (a) ferrite solid solution matrix, (b) Cr-rich $M_{23}C_6$ carbide, (c) $Fe_2Mo$ based Laves phase, and (d) V-, Nb-rich MX carbo-nitride.

T91 steel chemical composition is to be around 640 ℃.

The phase diagram in Fig. 6a shows the effect of temperature and Mo-content on the phase composition of T91 steel, whereas Fig. 6b demonstrates the effect of temperature and C-content on the T91 steel phase composition.

In Fig. 6a it is demonstrated that with decreasing temperature, the solubility of Mo in ferrite solid solution is decreasing which gives rise to an increase of precipitation amount of $Fe_2Mo$ Laves phase. On the other hand, Fig. 6b shows that with decreasing temperature, the solubility of C in both the austenite and ferrite solid solutions is decreasing which gives rise to an increase of precipitation amounts of $Cr_{23}C_6$ based carbides. Moreover, the temperature dependence of the carbon solubility within the ferrite is far much steeper (Fig. 6b) than the temperature dependence of the molybdenum solubility (Fig. 6a). Therefore, the differences in the amounts of $Cr_{23}C_6$ carbide precipitates in both long-term aged material states (600 ℃/5000 h and 650 ℃/5000 h) are rather negligible (Fig. 4). By summary, a thermodynamic calculation in Fig. 6c shows the calculated mole fractions of stable phases for the fixed chemical composition of T91 steel depending on temperature. Since according to Fig. 6c the equilibrium amount of brittle intermetallic Laves phase precipitates at 600 ℃ is very low, i.e., below 0.01 mole fraction and at 650 ℃ even 0 mole fraction, the tendency of T91 steel to thermally-induced embrittlement can be expected to be very low or none.

Figure 7 shows the values of CVN impact toughness for individual heat-treated material states in conditions without and with hydrogen charging.

The results show that neither the long-term ageing nor electrochemical hydrogenation induced any significant changes in obtained values of CVN impact toughness. This observation clearly demonstrates excellent brittle fracture resistance of T91 steel in both the long-term aged and hydrogen-charged material states at

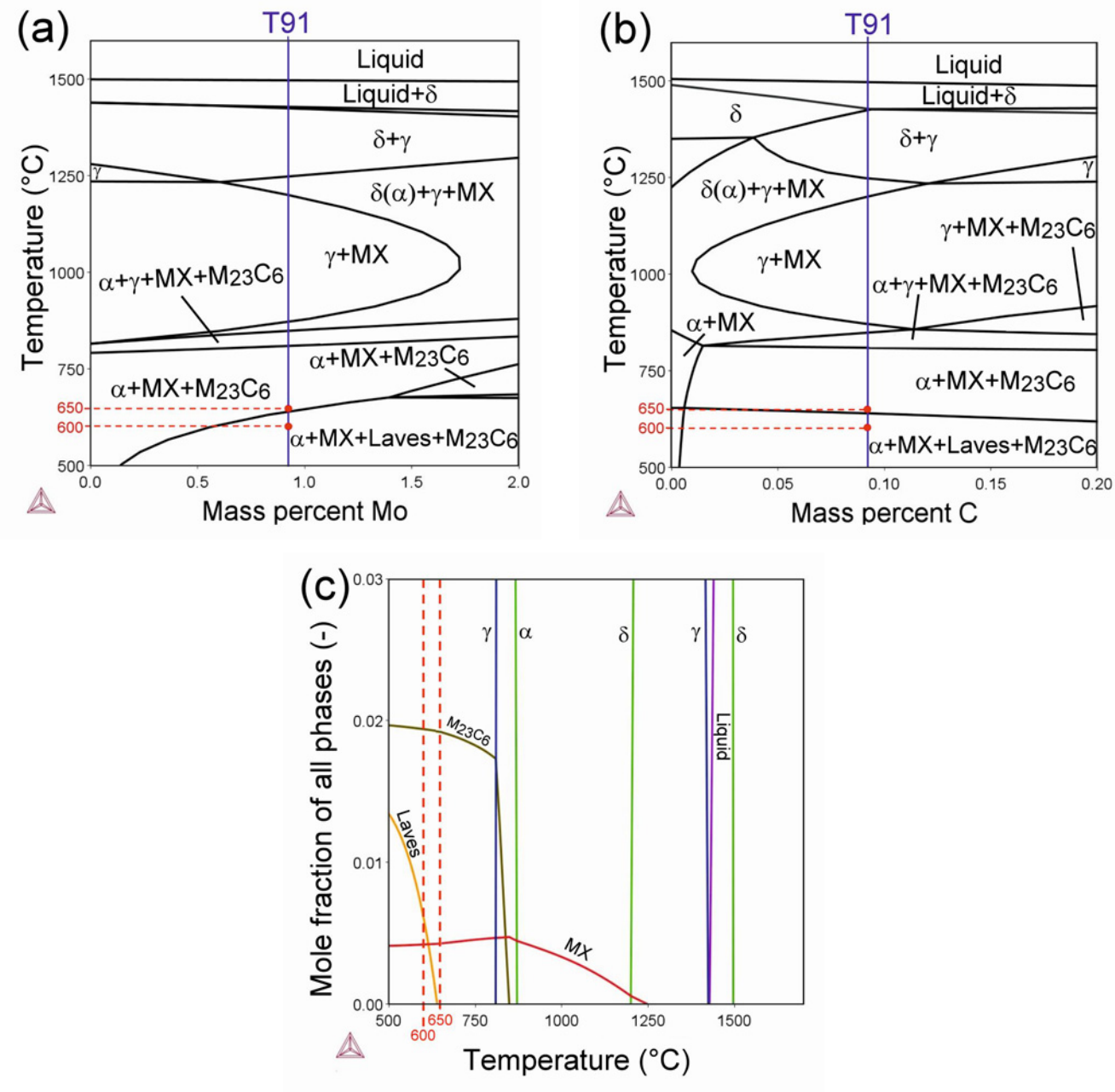


Fig. 6. Calculated phase diagrams showing the occurrence of thermodynamically stable phases for T91 steel: (a) dependence on temperature and Mo-content, (b) dependence on temperature and C-content, and (c) temperature dependence at fixed T91 steel composition.

room-temperature impact loading conditions. In order to quantitatively differentiate between the effects of long-term ageing, hydrogen charging, and their mutual superposition on the resulting brittle fracture resistance, calculated $EI_{CVN}$ values are presented in Table 2. The values of embrittlement index were calculated according to the Eq. (1) using the mean CVN impact toughness values related to individual material conditions as shown in Fig. 7.

Although both the positive and negative $EI_{CVN}$ values representing either embrittling or toughening behaviors have been obtained (Table 2), the overall $EI_{CVN}$ values variation is rather small. The reason for the observed slight toughening effect (i.e. negative $EI_{CVN}$ value) induced by long-term ageing and hydrogen charging after long-term ageing of T91 steel at 650 ℃ is not completely understood at this point of investigation. It is assumed that some thermally--induced toughening effects might be induced by the occurred spheroidization of the finest semi-coherent precipitates leading to the material softening. Due to additional precipitation of fine precipitates during

Table 2. Embrittlement index ($EI_{CVN}$) for individual material states of T91 steel

| Row | Initial state | Final state | $EI_{CVN}$ (%) |
|---|---|---|---|
| 1 | N&T | N&T + H | 4.1 |
| 2 | N&T + 600 °C/5000 h | N&T + 600 °C/5000 h + H | 2.0 |
| 3 | N&T + 650 °C/5000 h | N&T + 650 °C/5000 h + H | –6.6 |
| 4 | N&T | N&T + 600 °C/5000 h | –0.6 |
| 5 | N&T | N&T + 650 °C/5000 h | –2.0 |
| 6 | N&T | N&T + 600 °C/5000 h + H | 1.4 |
| 7 | N&T | N&T + 650 °C/5000 h + H | –8.7 |

Rows 1–3: hydrogen (H) charging effects; Rows 4,5: long-term ageing effects; Rows 6,7: superposition of long-term ageing and H charging effects.

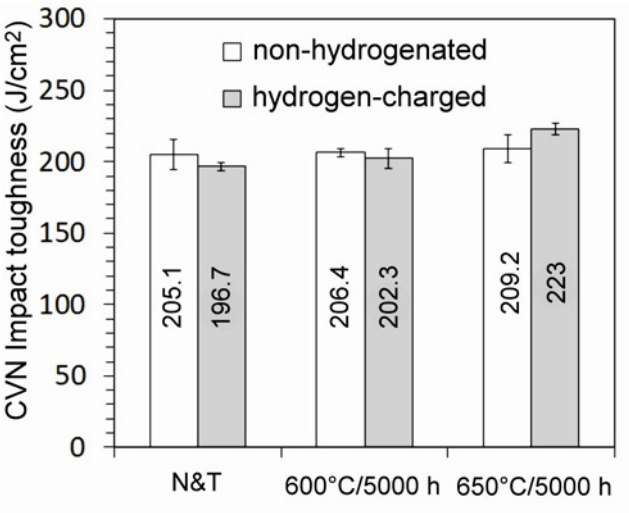


Fig. 7. Effect of long-term ageing and hydrogen charging on CVN impact toughness.

thermal exposure, the number of irreversible hydrogen traps is increased and by this way the amount of free diffusible hydrogen is decreased [32]. Moreover, as the grain boundaries are generally considered the reversible (i.e. weak) hydrogen trapping sites increasing the hydrogen embrittlement (HE) susceptibility, the observed grain growth during long-term ageing accompanied by overall reduction of grain boundary area could also result in observed slight increase of the HE resistance. Pandey et al. [16] also observed the decreasing EI values with increasing diffusible hydrogen level in P91 steel weld deposit. It is generally accepted that the grade 91 steel is prone to HE under quasi-static loading conditions, especially in as-welded or insufficiently tempered material condition due to its sharp martensitic lath microstructure [33]. However, after the quality N&T treatment and especially after long-term ageing inducing further microstructure tempering, the resistance to HE may even slightly increase, which has also been demonstrated by the results obtained in present investigation.

Figure 8 shows the SEM images of fracture surfaces of broken CVN impact toughness test specimens related to individual material states of investigated T91 steel after performing the room-temperature Charpy impact bending tests.

The observed fracture micro-mechanisms are represented by a mixture of both the ductile dimple tearing (i.e. micro-void coalescence fracture) representing the major fracture part and minor portion of transgranular quasi-cleavage (mainly around non-metallic inclusions) for all the studied material conditions which corresponds well with the obtained values of CVN impact toughness (Fig. 7). This mechanical and fracture behavior indicates very good brittle fracture resistance of the long-term aged and hydrogen-charged T91 heat-resistant steel in impact loading conditions.

## 4. Summary and conclusions

In this study brittle fracture resistance of T91 heat-resistant steel was investigated in long-term aged and cathodically hydrogen-charged material conditions. The obtained results are summarized in following conclusions:

– Microstructural investigations of individual material states revealed that all studied microstructures are composed of tempered martensitic structures consisting of ferritic matrix, $Cr_{23}C_6$ based carbides and (V,Nb)(C,N) carbo-nitrides.

– Compared to the initial N&T and long-term aged 650 °C/5000 h material states, the 600 °C/5000 h aged material exhibited additional precipitation and coarsening of a very little amount of intermetallic $Fe_2Mo$ based Laves phase to be below 0.01 mole fraction with respect to performed thermodynamic calculation.

– In accordance with performed thermodynamic predictions, the amounts of individual secondary phase precipitates were slightly increasing with decreasing ageing temperature due to the decreasing solubility limits of alloying elements in the ferritic matrix with decreasing temperature.

– The obtained results of room-temperature Char-

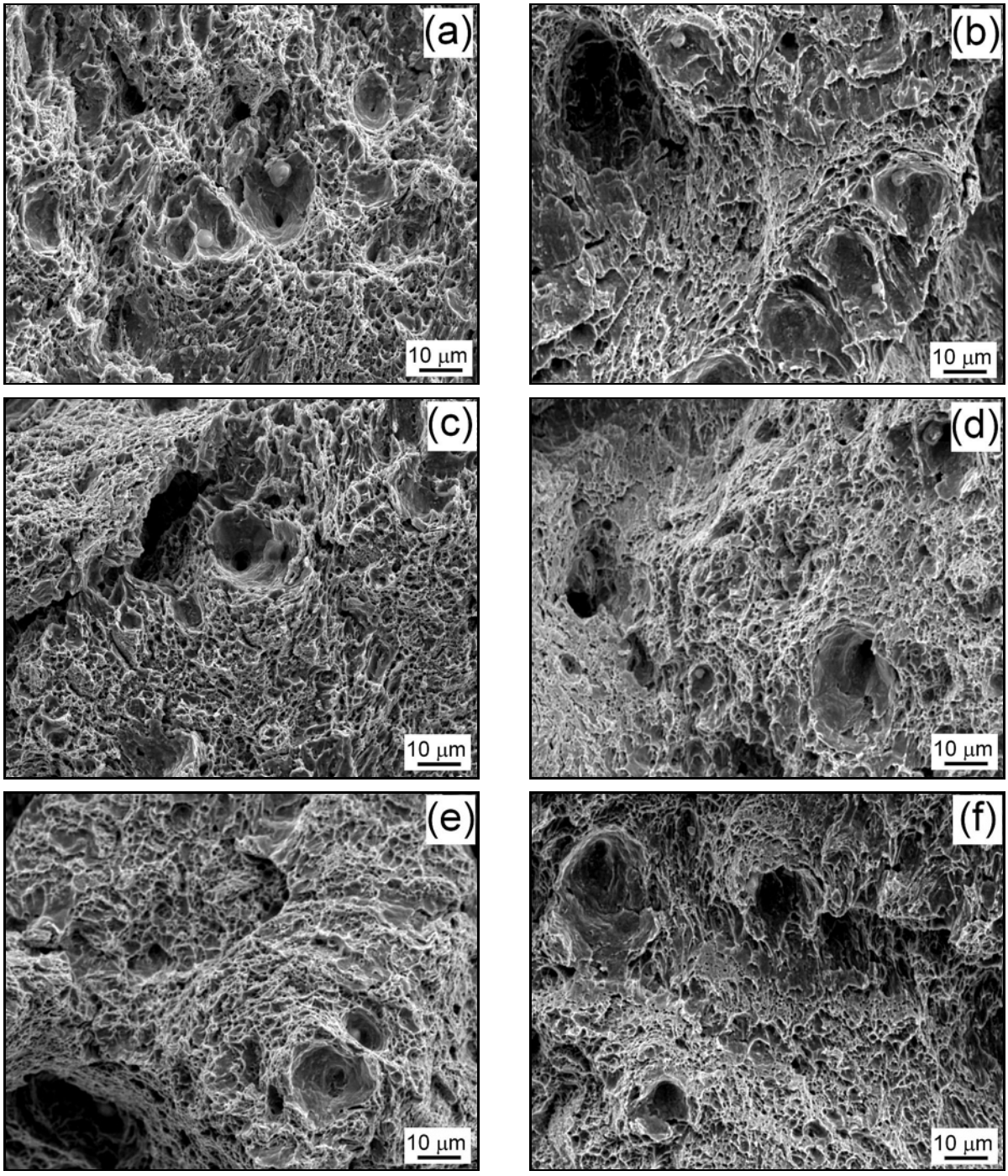


Fig. 8. SEM images of fracture surfaces of broken CVN impact toughness specimens related to individual material states of T91 steel under investigation: (a) N&T state, (b) N&T state with hydrogen, (c) 600 °C/5000 h state, (d) 600 °C/5000 h state with hydrogen, (e) 650 °C/5000 h state, and (f) 650 °C/5000 h state with hydrogen.

py impact bending tests indicated similar CVN impact toughness values for all the studied material conditions, i.e. the effects of both the long-term ageing and hydrogen charging on the resulting brittle-fracture resistance of T91 steel under investigation were rather small.

– The revealed excellent brittle fracture resistance of T91 steel can be related to its optimal alloying and microstructural characteristics, namely its stable, highly tempered martensitic microstructure and very low volume fraction of intermetallic Laves phase not compromising the toughness of the material.

## Acknowledgements

This work was supported by the Slovak Research and

Development Agency under the contract No. APVV-23-0034. The conducted research was also performed within the frame of the project supported by the Slovak National Grant Agency, grant No. VEGA 2/0069/24. The authors are grateful to Dr. A. Kroupa (IPM ASCR, Brno, Czech Republic) for the possibility of using his developed non-commercial thermodynamic database STEEL16 in currently performed thermodynamic calculations of T91 steel phase composition.

## References

[1] V. K. Sikka, C. T. Ward, K. C. Thomas, Modified 9Cr-1Mo steel, In: Proc. Conf. on Ferritic Steels for High Temperature Applications. Warren, PA: ASM (1981) 65–84.

[2] C. Pandey, N. Saini, M. M. Mahapatra, P. Kumar, Study of the fracture surface morphology of impact and tensile tested cast and forged (C&F) Grade 91 steel at room temperature for different heat treatment regimes, Engineering Failure Analysis 71 (2017) 131–147. https://doi.org/10.1016/j.engfailanal.2016.06.012

[3] R. Bonetti, N. C. Neate, A. Morris, P. H. Shipway, W. Sun, Microstructure evolution and deformation mechanisms of service-exposed P91 steel via interrupted uniaxial creep tests at 660 °C, Journal of Materials Research and Technology 33 (2024) 3529–3549. https://doi.org/10.1016/j.jmrt.2024.10.045

[4] B. S. Dutt, M. N. Babu, G. Shanthi, P. K. Parida, A. Moitra, M. Vasudevan, Effect of long term aging on fracture resistance of modified 9Cr-1Mo (P91) steel, Journal of Materials Engineering and Performance 35 (2025) 10308–10324. https://doi.org/10.1007/s11665-025-12969-7

[5] S. K. Mohanty, S. Behera, C. Pandey, K. Guguloth, Creep deformation behaviour of Grade 91 steel and its weld joints: A comparative study, International Journal of Pressure Vessels and Piping 219 (2026) 105678. https://doi.org/10.1016/j.ijpvp.2025.105678

[6] Y.-C. Feng, J.-X. Ren, J.-P. Liu, Z.-M. Gu, M. Zhong, C. Wang, Impact toughness dependence upon post-weld cooling temperature in P91 steel weldments, Journal of Iron and Steel Research International 32 (2025) 4006–4012. https://doi.org/10.1007/s42243-025-01458-9

[7] M. Ni, J. Wang, J. Liu, X. Wang, K. Zhang, C. Du. Microstructure and mechanical properties of P91 Steel during heat treatment: The effect of the cooling speed during the normalization stage, Journal of Materials Engineering and Performance 30 (2021) 2329–2340. https://doi.org/10.1007/s11665-021-05534-5

[8] A. Grybėnas, V. Makarevičius, A. Baltušnikas, I. Lukošiūtė, R. Kriūkienė, Correlation between structural changes of $M_{23}C_6$ carbide and mechanical behaviour of P91 steel after thermal aging, Materials Science and Engineering: A 696 (2017) 453–460. https://doi.org/10.1016/j.msea.2017.04.103

[9] L. Zhu, X. Liu, P. Fan, Y. Yang, K. Zhang, K. Wang, L. Wang, Evaluation of microstructure degradation during creep of P91 steel using electrochemical detection technique, Materials Today Communications 34 (2023) 105039. https://doi.org/10.1016/j.mtcomm.2022.105039

[10] V. Vodárek, J. Holešinský, Z. Kuboň, R. Palupčíková, P. Váňová, J. Malcharcziková, Creep resistance and microstructure evolution in P23/P91 welds, Materials 18 (2025) 194. https://doi.org/10.3390/ma18010194

[11] S. Kumar, S. Sirohi, J.G. Thakare, B. Adhithan, C. Pandey, Role of Mo in the nucleation of intermetallic laves phase, Materials Today: Proceedings 38 (2021) 2781–2791. https://doi.org/10.1016/j.matpr.2020.08.734

[12] J. Blach, L. Falat, P. Ševc, Fracture characteristics of thermally exposed 9Cr-1Mo steel after tensile and impact testing at room temperature, Engineering Failure Analysis 16 (2009) 1397–1403. https://doi.org/10.1016/j.engfailanal.2008.09.003

[13] H. Zhao, Z. Wang, X. Han, M. Wang, Effect of long-term aging on the microstructural evolution in a P91 steel, Materials 15 (2022) 2847. https://doi.org/10.3390/ma15082847

[14] Z.-X. Xia, C.-Y. Wang, Y.-F. Zhao, G.-D. Zhang, L. Zhang, X.-M. Meng, Laves phase formation and its effect on mechanical properties in P91 steel, Acta Metallurgica Sinica (English Letters) 28 (2015) 1238–1246. https://doi.org/10.1007/s40195-015-0318-5

[15] S. G. Sarwat, J. Basu, Understanding Laves phase precipitation induced embrittlement of modified 9Cr–1Mo steel, SN Applied Sciences 1 (2019) 89. https://doi.org/10.1007/s42452-018-0101-0

[16] C. Pandey, N. Saini, M. M. Mahapatra, P. Kumar. Hydrogen induced cold cracking of creep resistant ferritic P91 steel for different diffusible hydrogen levels in deposited metal, International Journal of Hydrogen Energy 41(39) (2016) 17695–17712. https://doi.org/10.1016/j.ijhydene.2016.07.202

[17] J. Blach, L. Falat, The influence of thermal exposure and hydrogen charging on the notch tensile properties and fracture behaviour of dissimilar T91/TP316H weldments, High Temperature Materials and Processes 33 (2014) 329–337. https://doi.org/10.1515/htmp-2013-0053

[18] X. Sun, C. Che, G. Qian, X. Wang, Microstructure, hardness and creep properties for P91 steel after long-term service in a ultra-supercritical power plant, International Journal of Pressure Vessels and Piping 212 (2024) 105330. https://doi.org/10.1016/j.ijpvp.2024.105330

[19] L. Marchetti, E. Herms, P. Laghoutaris, J. Chêne, Hydrogen embrittlement susceptibility of tempered 9%Cr–1%Mo steel. International Journal of Hydrogen Energy 36 (2011) 15880–15887. https://doi.org/10.1016/j.ijhydene.2011.08.096

[20] C. Hurtado Noreña, P. Bruzzoni, Effect of microstructure on hydrogen diffusion and trapping in a modified 9%Cr–1%Mo steel, Materials Science and Engineering: A 527 (2010) 410–416. https://doi.org/10.1016/j.msea.2009.08.025

[21] M. Rhode, T. Richter, T. Mente, P. Mayr, A. Nitsche, Thickness and microstructure effect on hydrogen diffusion in creep-resistant 9% Cr P92 steel and P91 weld metal, Weld World 66 (2022) 325–340. https://doi.org/10.1007/s40194-021-01218-9

[22] G. Junak, J. Adamiec, K. Łyczkowska, Mechanical properties of P91 steel (X10CrMoVNb9-1) during simulated operation in a hydrogen-containing environment, Materials 17 (2024) 4398. https://doi.org/10.3390/ma17174398

[23] S. K. Bonagania, B. Vishwanadh, S. Tenneti, N. N. Kumar, V. Kain, Influence of tempering treatments on mechanical properties and hydrogen embrittlement of 13 wt% Cr martensitic stainless steel, International Journal of Pressure Vessels and Piping 176 (2019) 103969. https://doi.org/10.1016/j.ijpvp.2019.103969
[24] M. Cauwels, R. Depraetere, W. De Waele, S. Hertelé, K. Verbeken, T. Depover, Effect of hydrogen charging on Charpy impact toughness of an X70 pipeline steel, Procedia Structural Integrity 42 (2022) 977–984. https://doi.org/10.1016/j.prostr.2022.12.123
[25] A. M. Kpemou, G. Pluvinage, J. Capelle, Influence of hydrogen embrittlement on ductile-brittle transition temperature determined on mini-charpy specimens made in X65 steel, Journal of Failure Analysis and Prevention 21 (2021) 2290–2304. https://doi.org/10.1007/s11668-021-01286-5
[26] L. Falat, L. Čiripová, O. Petruš, V. Puchý, I. Petryshynets, K. Kovaľ, R. Džunda, The effects of electrochemical hydrogen charging on charpy impact toughness and dry sliding tribological behavior of AISI 316H stainless steel, Crystals 13 (2023) 1249. https://doi.org/10.3390/cryst13081249
[27] X. Guo, J. Gong, Y. Jiang, D. Rong, The influence of long-term aging on microstructures and static mechanical properties of P92 steel at room temperature, Materials Science and Engineering: A 564 (2013) 199–205. https://doi.org/10.1016/j.msea.2012.10.024
[28] I. Fedorova, A. Belyakov, P. Kozlov, V. Skorobogatykh, I. Shenkova, R. Kaibyshev, Laves-phase precipitates in a low-carbon 9% Cr martensitic steel during aging and creep at 923 K, Materials Science and Engineering: A 615 (2014) 153–163. https://doi.org/10.1016/j.msea.2014.07.046
[29] L. Maddi, G. S. Deshmukh, A. R. Ballal, D. R. Peshwe, R. K. Paretkar, K. Laha, M. D. Mathew, Effect of Laves phase on the creep rupture properties of P92 steel, Materials Science and Engineering: A 668 (2016) 215–223. https://doi.org/10.1016/j.msea.2016.05.074
[30] M. Junek, M. Svobodova, J. Horvath, V. Mara, The effect of long-term ageing on microstructural properties and laves phase precipitation of welded P91and P92 steels, Steel Research International (2021) 2100311. https://doi.org/10.1002/srin.202100311
[31] H. Salama, J. Kundin, O. Shchyglo, V. Mohles, K. Marquardt, I. Steinbach, Role of inclination dependence of grain boundary energy on the microstructure evolution during grain growth, Acta Materialia 188 (2020) 641–651. https://doi.org/10.1016/j.actamat.2020.02.043
[32] X. Y. Cheng, H. Li, X. B. Cheng, Carbides and possible hydrogen irreversible trapping sites in ultrahigh strength round steel, Micron 103 (2017) 22–28. https://doi.org/10.1016/j.micron.2017.09.005
[33] M. Rhode, J. Nietzke, T. Richter, T. Mente, P. Mayr, A. Nitsche, Hydrogen effect on mechanical properties and cracking of creep-resistant 9% Cr P92 steel and P91 weld metal, Weld World 67 (2023) 183–194. https://doi.org/10.1007/s40194-022-01410-5